NASA Technical Memorandum 4436

Characterization of Cavity Flow Fields Using Pressure Data Obtained in the Langley 0.3-Meter Transonic Cryogenic Tunnel

M. B. Tracy and E. B. Plentovich

MARCH 1993

NASA Technical Memorandum 4436

Characterization of Cavity Flow Fields Using Pressure Data Obtained in the Langley 0.3-Meter Transonic Cryogenic Tunnel

M. B. Tracy and E. B. Plentovich
Langley Research Center
Hampton, Virginia

Abstract

Static and fluctuating pressure distributions were obtained along the floor of a rectangular-box cavity in an experiment performed in the Langley 0.3-Meter Transonic Cryogenic Tunnel. The cavity studied was 11.25 in. long and 2.50 in. wide with a variable height to obtain length-to-height ratios of 4.4, 6.7, 12.67, and 20.0. The data presented herein were obtained for yaw angles of 0° and 15° over a Mach number range from 0.2 to 0.9 at a Reynolds number of 30 × 10^6 per foot with a boundary-layer thickness of approximately 0.5 in. The results indicated that open and transitional-open cavity flow supports tone generation at subsonic and transonic speeds at Mach numbers of 0.6 and above. Further, pressure fluctuations associated with acoustic tone generation can be sustained when static pressure distributions indicate that transitional-closed and closed flow fields exist in the cavity. Cavities that support tone generation at 0° yaw also supported tone generation at 15° yaw when the flow became transitional-closed. For the latter cases, a reduction in tone amplitude was observed. Both static and fluctuating pressure data must be considered when defining cavity flow fields, and the flow models need to be refined to accommodate steady and unsteady flows.

Introduction

Cavities in aerodynamic surfaces can generate both steady and unsteady disturbances in otherwise uniform flow fields. Changes in static pressure distributions inside the cavity can result in large pressure gradients, and the unsteady flow can generate self-sustaining oscillations which, in turn, generate acoustic tones that radiate from the cavity. Both steady and unsteady flows can present difficulties for store separation from an internal weapons bay. The former can cause large nose-up pitching moments, and the latter can cause structural vibration of the store. To ensure safe separation, the various flow fields that develop about a cavity must be characterized. The experimental and computational results from studies of the mean flow field within a cavity have been reported in references 1–14. Cavity acoustic results have been reported in references 1, 2, 6, and 15–27.

The purpose of this study is to characterize the cavity flow fields observed at subsonic and transonic speeds by using the complimentary static and fluctuating pressure data measured along the length of the cavity. Previous publications (refs. 28 and 29) separately analyzed the static and fluctuating pressure data obtained in this experiment for the effects of Reynolds number and yaw angle, and they found no significant effect due to Reynolds number (separate from boundary-layer thickness) in either the static or the fluctuating pressure data. The static results indicated that the various types of flow fields occurred for length-to-height ratios (l/h) that were different from those observed at supersonic speeds. Specifically, the cavity with $l/h = 6.7$, which would support open flow at supersonic speeds, showed transitional-open flow at a free-stream Mach number (M_∞) of 0.6 and tended toward open flow as the Mach number was increased to 0.9. The cavity with $l/h = 12.67$, which would support transitional flow at supersonic speeds, showed closed flow at $M_\infty = 0.6$ and tended toward transitional-closed as the Mach number was increased to 0.9. The acoustic results, based on fluctuating pressures measured at a single location on the forward floor of the cavity, agreed with supersonic observations in most cases. A notable exception was the cavity with $l/h = 12.67$ in which tones developed when the Mach number was reduced to 0.6. The tone amplitude and bandwidth were observed to change from transonic through subsonic with decreasing Mach number for all cases for which tones occurred.

The intention of this study is to extend the analysis to more thoroughly characterize the various flow fields and the transitions between them at subsonic and transonic speeds. Some previously published data (acoustic spectra and static pressure distributions) are presented to demonstrate both the cases for which static and fluctuating pressure data were consistent and the cases for which they were not. Additional unpublished acoustic data measured along the cavity floor are used to generate mode shape plots.

Symbols and Abbreviations

BLC	boundary-layer control
C_p	pressure coefficient, $\frac{p_s - p_\infty}{q_\infty}$
D	diameter, ft
f_m	frequency of acoustic mode, Hz
h	cavity height, in.
k	empirical ratio of shear layer and free-stream velocities, a function of M_∞
LN_2	liquid nitrogen
l	cavity length, in.
M_∞	free-stream Mach number
m	acoustic mode number
N_2	nitrogen
p_f	measured fluctuating pressure, psi
p_s	measured surface static pressure, psi
$p_{t,\infty}$	free-stream total pressure, psi
p_∞	free-stream static pressure, psi
q_∞	free-stream dynamic pressure, psi
R_∞	free-stream unit Reynolds number, per ft
SPL	sound pressure level, dB
$T_{t,\infty}$	free-stream total temperature, K
U_∞	free-stream velocity, fps
x	distance in streamwise direction, in.
y	distance in spanwise direction, in.
z	distance normal to tunnel sidewall, in.
α	empirical phase between instabilities in shear layer and pressure waves, a function of l/h
γ	ratio of specific heat of test gas at constant pressure to that at constant volume
δ	boundary-layer thickness, in.
δ^*	boundary-layer displacement thickness, in.
θ	boundary-layer momentum thickness, in.
ψ	yaw angle, deg

Background

At supersonic speeds, four types of mean cavity flow were defined in references 13 and 14, and these four types (open, closed, transitional-closed, and transitional-open) will be briefly discussed. The first flow type generally occurs when the cavity is deep, as found in bomb bays, and is termed *open cavity flow.* This flow type generally occurs for $l/h \leq 10$ at supersonic speeds. Sketches of the open cavity flow field and typical pressure distributions are shown in figure 1. For open cavity flow, the flow essentially bridges the cavity and a shear layer is formed over the cavity (fig. 1(a)). A weak shock wave can form near the leading edge of the cavity as a result of the flow being compressed slightly by the shear layer. A nearly uniform static pressure distribution is produced where the cavity flow is open (fig. 1(b)), which is desirable for safe store separation; however, high-intensity acoustic tones can develop (fig. 1(c)). These tones can induce vibrations in the surrounding structure, including the separating store, and lead to structural fatigue.

The second type of cavity flow is found with shallow cavities and is termed *closed cavity flow.* The cavity configurations typical of missile bays on fighter aircraft are shallow cavities. At supersonic speeds, closed cavity flow generally occurs for $l/h \geq 13$. Figure 2 provides a sketch of the flow field and typical pressure distributions for closed cavity flow. In this flow type, the flow separates at the forward face of the cavity, reattaches at some point along the cavity floor, and then separates again before reaching the rear cavity face (fig. 2(a)). This creates two distinct separation regions, one downstream of the forward face and one upstream of the rear face. This flow produces an adverse static pressure gradient (fig. 2(b)) that can cause the separating store to experience large nose-up pitching moments. However, acoustic tones are not present for shallow cavities where the flow is closed.

The third and fourth mean cavity flow types (transitional-closed and transitional-open) occur for cavities with values of l/h that fall between those for closed cavity flow and open cavity flow, (i.e., values of l/h between 10 and 13). *Transitional-closed cavity flow* in the past has been referred to as transitional cavity flow (ref. 4); however, the impingement shock and the exit shock that normally occur for closed cavity flow coincide and produce

a single shock as shown in figure 3(a). Similar to the result for closed cavity flow, large longitudinal pressure gradients occur (fig. 3(b)) in the cavity that can contribute to large nose-up pitching moments.

With a small reduction in l/h from a value corresponding to transitional-closed cavity flow, the impingement-exit shock wave abruptly changes to a series of expansion and compression wavelets indicating that the shear layer no longer impinges on the cavity floor. This flow field is referred to as *transitional-open cavity flow*. For this flow field, as indicated in figure 3(c), longitudinal pressure gradients in the cavity are not as large as those shown for transitional-closed cavity flow (fig. 3(d)), and consequently the problem of store nose-up pitching moment is not as severe as that for closed cavity flow. The acoustic fields corresponding to the transitional flow fields have not been determined.

The mechanism that produces acoustic tones for open cavity flow fields is understood to be a reinforcement between instabilities in the shear layer that bridges the cavity and pressure waves that are generated in the cavity when the shear layer impinges on the aft wall. Acoustic tones occur at discrete frequencies that correspond to characteristic pressure patterns (standing waves or modes) in the cavity. Although no satisfactory method exists to predict tone amplitude, the frequencies at which they occur can be predicted by a semiempirical equation determined by Rossiter in reference 1 and modified by Heller, Holmes, and Covert in reference 15. The modified Rossiter equation is given as

$$f_m \frac{l}{U_\infty} = \frac{m - \alpha}{M_\infty \left[1 + (\frac{\gamma-1}{2}) M_\infty^2\right]^{-1/2} + \frac{1}{k}} \qquad (1)$$

The determination of transitional-closed and transitional-open cavity flows, as well as of open and closed cavity flows, has been made by observation of the static pressure distribution in the cavity. Figures 1(b), 2(b), 3(b), and 3(d) provide typical static pressure distributions for each flow type that can be used as a guideline for determining the type of cavity flow.

Cavity flow regimes are generally defined in terms of the length-to-height ratio of the cavity. However, there are other parameters that can affect the exact value of l/h where the flow transitions from closed to open. Some of these parameters include Mach number (ref. 1), the ratio of cavity width to cavity height (ref. 4), and the ratio of boundary-layer height to cavity height (ref. 3). Cavity parameters and free-stream conditions should match when making data comparisons.

Experimental Methods

Wind Tunnel Description

The tests were conducted in the 13- by 13-in. adaptive-wall test section of the Langley 0.3-Meter Transonic Cryogenic Tunnel (0.3-m TCT). A sketch of the tunnel is presented in figure 4. The 0.3-m TCT is a fan-driven, cryogenic pressure tunnel that uses gaseous nitrogen as a test medium. It is capable of operating at stagnation temperatures from approximately 80 K to 327 K and at stagnation pressures from 1.2 to 6.0 atm. The fan speed is variable so that the empty test section Mach number can be varied continuously from about 0.20 to 0.95. This combination of test conditions provides a test envelope of Reynolds numbers up to about 100×10^6 per foot. Additional details of the tunnel and its range of operation may be found in references 30 and 31.

Figure 5 presents a sketch showing details of the flow region in the adaptive-wall test section, and figure 6 presents a photograph of the test section. All four walls are solid. The sidewalls are rigid, whereas the top and bottom walls are flexible and movable. The flexible top and bottom walls are computer controlled, with feedback provided on the wall positions and pressure distributions to achieve alignment with model streamlines. This produces flow in the vicinity of the model that approaches the flow which would be obtained for free-air conditions. Specific information on the adaptive-wall test section and a brief description of the strategy used to contour the walls can be found in reference 32.

Model Description

A rectangular cavity model was mounted on a turntable installed in the sidewall of the 0.3-m TCT to produce an angle of attack of 0°. Figure 7 shows the cavity with pressure instrumentation prior to installation in the tunnel. The cavity was 2.50 in. wide by 11.25 in. long and the height was varied to obtain l/h ratios of 4.4 (h = 2.56 in.), 6.7 (h = 1.68 in.), 12.67 (h = 0.89 in.), and 20.0 (h = 0.56 in.). The turntable could be rotated with respect to the flow to position the cavity with a yaw angle of 0° and 15°.

The model was instrumented with 18 static pressure orifices and 19 flush-mounted dynamic pressure transducers. Sixteen of the dynamic pressure transducers were mounted along the centerline (13 on the cavity floor and 3 on the tunnel sidewall adjacent to

the cavity), 1 each on the fore and aft walls at half-depth and an additional sealed transducer on the cavity floor. The instrumentation layout is shown in figure 8. Table I provides the measured positions of the static pressure orifices and table II provides the measured positions of the dynamic pressure transducers.

Test Conditions

The model was tested in the 0.3-m TCT at Mach numbers from 0.2 to 0.9, unit Reynolds numbers ranging from 2.0×10^6 to 100×10^6 per ft (free-stream total temperatures ranging from 105 K to 320 K), and yaw angles of 0° and 15° (the limits of the range of the turntable). The data presented in this report were obtained with a Reynolds number of 30×10^6 per ft and a nominal free-stream total temperature of 112 K. The boundary-layer thickness was approximately equal to 0.5 in. Details of the boundary-layer measurements and calculations are given in reference 28, and table III summarizes these calculated boundary-layer parameters. The boundary-layer measurements were not made at the nominal test conditions indicated in table IV because of tunnel time constraints. The flexible test section walls were set to a "streamlined" shape for each test condition.

Instrumentation

Surface static pressures. Because of the large changes in dynamic pressure over the operating range in the 0.3-m TCT (a factor of about 75), a high-precision capacitive-type transducer is used for pressure measurements. The electrical outputs from the transducers are connected to individual signal conditioners. The signal conditioners are set on autorange to keep the transducer signal within voltage limits for the data acquisition system for all pressure ranges. The transducers have a maximum range from -100 to 100 lb/in^2 and have an accuracy of ± 0.25 percent from 25 percent of negative full scale to 100 percent of positive full scale. Additional details of the 0.3-m TCT pressure instrumentation system can be found in reference 30.

For the experimental data reported herein, each orifice was sampled 40 times over a 1-sec period; these data were then averaged to produce the mean value for each data point.

Fluctuating pressures. The transducers were miniature, high-sensitivity, piezoresistive, differential dynamic pressure transducers with a full-scale range of ± 10 psid and a resonant frequency of 130 000 Hz. Transducer 8 was sealed to verify that the sensitivity of the transducer to vibration was negligible. In order to utilize the maximum sensitivity of the transducers, the static component of the pressure measurement was removed. This was done by using a differential pressure transducer with local static pressure as a reference (transducers 1–3 were connected to orifice 1, transducers 4–11 were connected to orifice 7, and transducers 12–14, 18, and 19 were connected to orifice 17) and AC coupling the instrumentation. A 1000-Hz bench calibration verified that the temperature compensation maintained a sensitivity that was within 10 percent of a reference sensitivity at 100 K. Analog data were recorded on two 14-channel FM tape recorders using medium band format at 30 in/sec (DC at 10 kHz). A sine wave calibration was applied to each dynamic pressure transducer several times throughout the test.

Data Analysis of Fluctuating Pressure

An antialiasing filter was applied at 5 kHz, and the analog data were sampled at 12.5 kHz. The digitized data were divided into 50 blocks (assumed independent) of 4096 points each. Each block was Fourier analyzed using a Hanning window, and the resulting spectra were averaged. This method produces a spectral estimate with a frequency resolution of 3 Hz and 95 percent confidence that the spectral estimate is within ± 1 dB of the true spectra based on a Chi-square distribution. Fluctuating pressure is given as the sound pressure level (SPL) in decibels (dB). Thus,

$$\mathrm{SPL} = 20 \log \left(\frac{p_f}{2.9 \times 10^{-9} \text{ psi}} \right) \qquad (2)$$

Discussion of Results

The static and fluctuating pressure data from this test were analyzed separately in references 28 and 29, respectively, and the present report focuses on correlating static and fluctuating pressure data. Data obtained for a given Reynolds number and free-stream total temperature were analyzed. The conditions of $R_\infty = 30 \times 10^6$ per ft and $T_{t,\infty} \approx 112$ K were chosen because the largest number of tests with different Mach numbers was obtained for each configuration at these conditions. Because Reynolds number was determined not to significantly affect the data, comparisons of static and fluctuating pressure data made at a single Reynolds number should be representative of the same data at other Reynolds numbers.

Table IV summarizes the results for $R_\infty = 30 \times 10^6$ per ft and $T_{t,\infty} \approx 112$ K reported in references 28

and 29. The identification of flow field types is based on static pressure measurements. Acoustic tones are identified in spectra obtained from the transducer installed in the most forward location in the cavity floor. Data for low-subsonic conditions, $M_\infty = 0.2$, will not be examined further because the data were shown to have significantly different flow characteristics from flows at $M_\infty = 0.6$ and above (refs. 28 and 33).

Static pressure data for $\psi = 0°$ gave the following results. Cavities with $l/h = 4.4$ and 20.0 showed the same flow types as would be seen at supersonic speeds open and closed, respectively. The cavity with $l/h = 6.7$ exhibited transitional-open flow for the Mach number range of 0.6 to 0.9. This differs from results at supersonic speeds for which a cavity with $l/h = 6.7$ would support open cavity flow. The cavity with $l/h = 12.67$ exhibited closed cavity flow at $M_\infty = 0.6$ and transitional-closed flow at $M_\infty = 0.8$ and 0.9. At supersonic speeds, a cavity with $l/h = 12.67$ would support transitional-closed flow.

The corresponding fluctuating pressure data showed the following at $\psi = 0°$. When static pressure data showed open cavity flow, acoustic tones were indicated. Figure 9 gives typical results for open cavity flow for $l/h = 4.4$, $M_\infty = 0.9$, and $\psi = 0°$. Tones were also indicated when transitional-open flow occurred. Typical transitional-open flow results are given in figure 10 for $l/h = 6.7, M_\infty = 0.8$, and $\psi = 0°$. Except for the $l/h = 12.67$ cavity configuration at $M_\infty = 0.6$, tones were not indicated for closed cavity flow. Figure 11 gives typical closed cavity results for $l/h = 20.0, M_\infty = 0.6$, and $\psi = 0°$ (figs. 11(a) and (b)) and atypical results for $l/h = 12.67, M_\infty = 0.6$, and $\psi = 0°$ (figs. 11(c) and (d)). The tones at 519, 1038, and 1557 Hz in figure 11(b) were generated by tunnel fan blades.

At $\psi = 15°$, the static pressure results from cavity centerline orifices showed the flow to be transitional-closed for cavities with $l/h = 4.4$ and 6.7. For $l/h = 12.67$, the flow was closed. Fluctuating pressure data indicated that tones were present except for $l/h = 12.67$ at $M_\infty = 0.8$ and 0.9.

Transitional-closed and closed flow types occurred for different configurations, both with and without tones. For cavities with $l/h = 4.4$ and 6.7 at $\psi = 15°$, the flow was transitional-closed and tones were present; for a cavity with $l/h = 12.67$ at $M_\infty = 0.8$ and 0.9 and $\psi = 0°$, the flow was transitional-closed but no tones were apparent. A comparison of transitional-closed data, both with and without tones, is given in figure 12. Closed cavity flow occurred with tones for $l/h = 12.67, M_\infty = 0.6$, and $\psi = 0°$ and 15° and without tones for $l/h = 20.0, M_\infty = 0.6$ to 0.9, and $\psi = 0°$ and for $l/h = 12.67, M_\infty = 0.8$ and 0.9, and $\psi = 15°$. (No data were taken for $l/h = 20.0$ and $\psi = 15°$.)

To further illuminate the various cavity flow fields, fluctuating pressure data obtained along the length of the cavity were examined. As described in references 15, 27, and 29, tones occurred at frequencies that corresponded to characteristic pressure patterns or mode shapes in the cavity. These mode shapes can be traced by plotting the amplitude of a given tone (from spectra measured at discrete locations) along the length of the cavity. The presence of tones can be verified by determining if the variation of amplitude of the peak along the length of the cavity matches the characteristic pattern for the given mode. Figure 13 gives six mode shapes of a cavity with $l/h = 6.7, M_\infty = 0.9$, and $\psi = 0°$. For reference, the static pressure distribution and acoustic spectra measured on the forward floor of the cavity are given in figure 14. The acoustic tones are indicated with an asterisk. The first five mode shapes are clearly delineated in figure 13, but the sixth mode shape is not resolved completely because of the limited number of transducers along the length of the cavity. Tones corresponding to all modes do not occur in all the spectra. Table V gives a summary of the modes that were present when tones occurred. Observed frequencies are given in table V and, for reference, table VI gives acoustic modal frequencies predicted by the modified Rossiter equation. (See eq. (1).) Figure 15 gives a plot of the predicted frequencies with the observed frequencies indicated.

Since the flow field depends on the value of l/h, a comparison of three mode shapes for different values of l/h was made for given Mach numbers at $\psi = 0°$. Figures 16, 17, and 18 give plots for modes 1, 2, and 3, respectively. Neither table V nor figures 16 to 18 provide any further definition of the flow field types. The only data available for comparison for closed cavity flow (see $l/h = 12.67$ data in fig. 18(a)) indicate that a third acoustic mode is present and lower in amplitude than corresponding data for open and transitional-open flows.

Comparisons made between mode shapes determined for cavities at the two yaw angles are more informative. Although the cavity is no longer aligned with the flow, characteristic mode shapes are observed in cavities at $\psi = 15°$. This is taken as evidence that a yaw angle of 15° is not sufficient to disturb the feedback mechanism in the cavity that sustains acoustic tone generation. As seen in table IV, significant differences exist in static pressure

distributions between the two yaw angles for most cavity geometries and flow conditions. Data for the first two modes are given in figures 19 and 20 for a cavity with $l/h = 4.4$ for given Mach numbers. Similar data are given in figures 21 and 22 for a cavity with $l/h = 6.7$. In the majority of cases in which the flow field changes from open or transitional-open to transitional-closed, a reduction occurs in mode amplitude throughout the cavity.

Concluding Remarks

Static and fluctuating pressure data were obtained along the floor of a rectangular-box cavity in an experiment performed in the Langley 0.3-Meter Transonic Cryogenic Tunnel. The cavity was 11.25 in. long and 2.50 in. wide with a variable height to obtain length-to-height ratios of 4.4, 6.7, 12.67, and 20.0. Data were obtained over a Mach number range from 0.2 to 0.9 for yaw angles of 0° and 15°. The unit Reynolds number was 30×10^6 per foot, and the boundary-layer thickness was approximately 0.5 in.

Flow field types were identified based on static pressure measurements, and acoustic tones were identified by peaks in fluctuating pressure spectra and characteristic mode shapes in the cavity. Correlation of static and dynamic data yielded both anticipated and unexpected results. Acoustic tone generation was observed for open and transitional-open cavity flows. In some cases transitional-closed and closed cavity flow sustained tone generation. Cavities that supported acoustic tone generation at a yaw angle (ψ) of 0° also supported tone generation at $\psi = 15°$ when the flow became transitional-closed. For these cases a reduction in mode amplitude was observed. It is significant that tones can occur for transitional-closed and closed cavity flows, which were previously thought to preclude each other.

Both static and fluctuating pressure data are evidently needed to define flow field types. Further study is needed to refine the flow field models to accommodate both steady and unsteady flows.

NASA Langley Research Center
Hampton, VA 23681-0001
February 3, 1993

References

1. Rossiter, J. E.: *Wind-Tunnel Experiment on the Flow Over Rectangular Cavities at Subsonic and Transonic Speeds.* R. & M. No. 3438, British Aeronautical Research Council, Oct. 1964.
2. Kaufman, Louis G., II; Maciulaitis, Algirdas; and Clark, Rodney L.: *Mach 0.6 to 3.0 Flows Over Rectangular Cavities.* AFWAL-TR-82-3112, U.S. Air Force, May 1983. (Available from DTIC as AD A134 579.)
3. Charwat, A. F.; Roos, J. N.; Dewey, F. C., Jr.; and Hitz, J. A.: An Investigation of Separated Flows—Part I: The Pressure Field. *J. Aeronaut. Sci.,* vol. 28, no. 6, June 1961, pp. 457–470.
4. Stallings, Robert L., Jr.; and Wilcox, Floyd J., Jr.: *Experimental Cavity Pressure Distributions at Supersonic Speeds.* NASA TP-2683, 1987.
5. Dix, Richard E.: *On Simulation Techniques for the Separation of Stores From Internal Installations.* SAE Tech. Paper Ser. 871799, Oct. 1987.
6. Heller, Hanno H.; and Bliss, Donald B.: *Aerodynamically Induced Pressure Oscillations in Cavities—Physical Mechanisms and Suppression Concepts.* Tech. Rep. AFFDL-TR-74-133, U.S. Air Force, Feb. 1975.
7. Baysal, O.; Srinivasan, S.; and Stallings, L., Jr.: Unsteady Viscous Calculations of Supersonic Flows Past Deep and Shallow Three-Dimensional Cavities. AIAA-88-0101, Jan. 1988.
8. Catalano, George D.: *Turbulent Flow Over an Embedded Rectangular Cavity.* AFATL-TR-86-73, U.S. Air Force, Feb. 1987. (Available from DTIC as AD A177 928.)
9. Om, Deepak: Navier-Stokes Simulation for Flow Past an Open Cavity. AIAA-86-2628, Oct. 1986.
10. Baysal, O.; and Stallings, R. L., Jr.: Computational and Experimental Investigation of Cavity Flowfields. AIAA-87-0114, Jan. 1987.
11. Suhs, N. E.: Computations of Three-Dimensional Cavity Flow at Subsonic and Supersonic Mach Numbers. AIAA-87-1208, June 1987.
12. Srinivasan, S.; Baysal, O.; and Plentovich, E. B.: Navier-Stokes Calculations of Transonic Flows Past Open and Transitional Cavities. *Advances and Applications in Computational Fluid Dynamics,* O. Baysal, ed., FED-Vol. 66, American Soc. of Mechanical Engineers, 1988, pp. 169–179.
13. Wilcox, Floyd J., Jr.: Experimental Measurements of Internal Store Separation Characteristics at Supersonic Speeds. *Store Carriage, Integration and Release,* Royal Aeronautical Soc., 1990, pp. 5.1–5.16.
14. Stallings, Robert L., Jr.; and Forrest, Dana K.: *Separation Characteristics of Internally Carried Stores at Supersonic Speeds.* NASA TP-2993, 1990.
15. Heller, H. H.; Holmes, G.; and Covert, E. E.: *Flow-Induced Pressure Oscillations in Shallow Cavities.* AFFDL-TR-70-104, U.S. Air Force, Dec. 1970. (Available from DTIC as AD 880 496.)
16. Bartel, H. W.; and McAvoy, J. M.: *Cavity Oscillation in Cruise Missile Carrier Aircraft.* AFWAL-TR-81-3036, U.S. Air Force, June 1981. (Available from DTIC as AD A108 610.)

17. Clark, Rodney L.: *Evaluation of F-111 Weapon Bay Aeroacoustic and Weapon Separation Improvement Techniques.* AFFDL-TR-79-3003, U.S. Air Force, Feb. 1979. (Available from DTIC as AD A070 253.)

18. Shaw, Leonard; Clark, Rodney; and Talmadge, Dick: F-111 Generic Weapons Bay Acoustic Environment. AIAA-87-0168, Jan. 1987.

19. Gates, Roger S.; Butler, Carroll B.; Shaw, Leonard L.; and Dix, Richard E.: Aeroacoustic Effects of Body Blockage in Cavity Flow. AIAA-87-2667, Oct. 1987.

20. Shaw, Leonard; and Banaszak, Dave: *Weapons Internal Carriage/Separation-"WICS" Aeroacoustic Research.* AFWAL-TM-86-243-FIBG, U.S. Air Force, Mar. 1987.

21. Dix, R. E.: *Weapons Internal Carriage and Separation at Transonic Conditions.* AEDC-TMR-89-P4, U.S. Air Force, Oct. 1989.

22. Tracy, Maureen B.; and Stallings, Robert L., Jr.: *Coupling of Acoustic Environment in Rectangular Cavity With Store Vibration Characteristics During Simulated Separation in Supersonic Flow.* NASA TP-2986, 1990.

23. Dix, Richard E.; and Butler, Carroll: *Cavity Aeroacoustics.* AFATL-TP-90-08, U.S. Air Force, June 1990. (Available from DTIC as AD A223 853.)

24. Shaw, Leonard L.; and Reed, Gus: *Supersonic Flow Induced Cavity Acoustics.* AFWAL-TM-85-210, U.S. Air Force, Dec. 1985.

25. Rockwell, D.; and Naudascher, E.: Review—Self-Sustaining Oscillations of Flow Past Cavities. *Trans. ASME, Ser. I: J. Fluids Eng.*, vol. 100, no. 2, June 1978, pp. 152–165.

26. Komerath, N. M.; Ahuja, K. K.; and Chambers, F. W.: Prediction and Measurement of Flows Over Cavities—A Survey. AIAA-87-0166, Jan. 1987.

27. Smith, D. L.; and Shaw, L. L.: *Prediction of the Pressure Oscillations in Cavities Exposed to Aerodynamic Flow.* AFFDL-TR-75-34, U.S. Air Force, Oct. 1975. (Available from DTIC as AD A018 518.)

28. Plentovich, E. B.; Chu, Julio; and Tracy, M. B.: *Effects of Yaw Angle and Reynolds Number on Rectangular-Box Cavities at Subsonic and Transonic Speeds.* NASA TP-3099, 1991.

29. Tracy, M. B.; Plentovich, E. B.; and Chu, Julio: *Measurements of Fluctuating Pressure in a Rectangular Cavity in Transonic Flow at High Reynolds Numbers.* NASA TM-4363, 1992.

30. Ladson, Charles L.; and Ray, Edward J.: *Evolution, Calibration, and Operational Characteristics of the Two-Dimensional Test Section of the Langley 0.3-Meter Transonic Cryogenic Tunnel.* NASA TP-2749, 1987.

31. Rallo, Rosemary A.; Dress, David A.; and Siegle, Henry J. A.: *Operating Envelope Charts for the Langley 0.3-Meter Transonic Cryogenic Wind Tunnel.* NASA TM-89008, 1986.

32. Mineck, Raymond E.: *Hardware and Operating Features of the Adaptive Wall Test Section for the Langley 0.3-Meter Transonic Cryogenic Tunnel.* NASA TM-4114, 1989.

33. Plentovich, E. B.: *Three-Dimensional Cavity Flow Fields at Subsonic and Transonic Speeds.* NASA TM-4209, 1990.

Table I. Location of Static Pressure Orifices on Cavity Floor

Orifice	x, in.	y, in.
1	0.350	0
2	2.050	↓
3	2.854	
4	3.658	
5	4.462	
6	5.266	
7	6.071	
8	6.874	
9	7.678	
10	8.482	
11	9.286	
12	10.090	
13	10.894	
14	.800	.5
15	.800	−.5
16	5.666	.5
17	10.486	.5
18	10.486	−.5

Table II. Location of Dynamic Pressure Transducers

Transducer	x, in.	y, in.	Location in model
1	0.800	0	Cavity floor
2	1.700	↓	↓
3	2.450		
4	3.254		
5	4.058		
6	4.862		
7	5.666	↓	
[a]8	5.666	−.5	
9	6.470	0	
10	7.274	↓	
11	8.078		
[b]12	8.882		
13	9.686		
14	10.490		↓
15	−.690		Tunnel sidewall, forward of cavity
16	−.230	↓	Tunnel sidewall, forward of cavity
17	0	.47	Half-depth, forward cavity wall
18	11.250	.47	Half-depth, aft cavity wall
19	11.800	0	Tunnel sidewall, aft of cavity

[a]Transducer sealed to determine vibration sensitivity.

[b]Transducer failed during test.

Table III. Boundary-Layer Parameters

[Data taken from ref. 28]

M_∞	R_∞, ft^{-1}	$p_{t,\infty}$, psi	$T_{t,\infty}$, K	δ, in.	δ^*, in.	θ, in.
0.6	30×10^6	33	115	0.512	0.063	0.045
.8	30	27	112	.494	.066	.043
.9	30	26	114	.491	.064	.041

Table IV. Nominal Test Matrix and Data Summary at $R_\infty = 30 \times 10^6$ per Foot

[Data taken from refs. 28 and 29]

			Results[a,b] for $\psi = 0°$ with l/h of—				Results[a,b] for $\psi = 15°$ with l/h of—		
M_∞	$p_{t,\infty}$, psi	$T_{t,\infty}$, K	4.40	6.70	12.67	20.00	4.40	6.70	12.67
0.2	79.7	109	a, e	a, e			c, e	c, e	
.6	31.6	111	a, f	b, f	d, f	d, e	c, f	c, f	d, f
.8	26.9	112	a, f	b, f	c, e	d, e	c, f	c, f	d, e
.9	25.8	114	a, f	b, f	c, e	d, e	c, f	c, f	d, e

[a]Static pressure data key:
- a open cavity flow
- b transitional-open cavity flow
- c transitional-closed cavity flow
- d closed cavity flow

[b]Fluctuating pressure data key:
- e no acoustic tones
- f acoustic tones

Table V. Frequencies Observed for Acoustic Modes

l/h	ψ, deg	M_∞	Observed frequencies, Hz, for—					
			Mode 1	Mode 2	Mode 3	Mode 4	Mode 5	Mode 6
4.4	0	0.6		290	485	675		
	15	.6			465	665		
	0	.8	185	385	595			
	15	.8	185	405	580			
	0	.9	170	435	695			
	15	.9	165	435	615			
6.7	0	0.6		295	505	730		
	15	.6		295	515	775		
	0	.8	185	385	605			
	15	.8	200	395	600			
	0	.9	150	395	685	945	1215	1480
	15	.9	155	430	620			
12.67	0	0.6			505			
	15	.6			505			

Table VI. Frequencies Predicted by Modified Rossiter Equation[a] for Acoustic Modes

[l=11.25 in.; $\gamma = 1.4$; $\alpha(l/h = 4) = 0.25$; $k(M_\infty = 0.4\text{–}1.2) = 0.57$]

M_∞	U_∞, fps	Predicted frequencies, Hz, for—					
		Mode 1	Mode 2	Mode 3	Mode 4	Mode 5	Mode 6
0.6	402.3	137	322	506	691	875	1060
.8	527.4	169	394	619	843	1069	1294
.9	589.0	182	427	666	911	1156	1395

[a] $$f_m \frac{l}{U_\infty} = \frac{m - \alpha}{M_\infty \left[1 + \left(\frac{\gamma - 1}{2}\right) M_\infty^2\right]^{-1/2} + \frac{1}{k}}$$

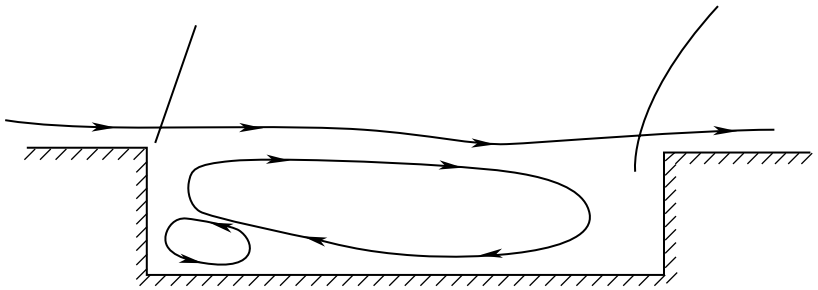

(a) Flow field model.

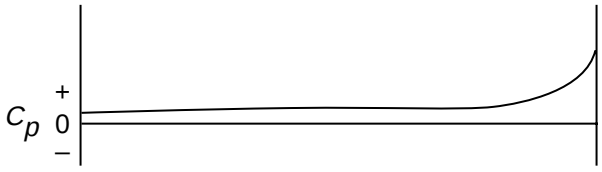

(b) Typical static pressure distribution.

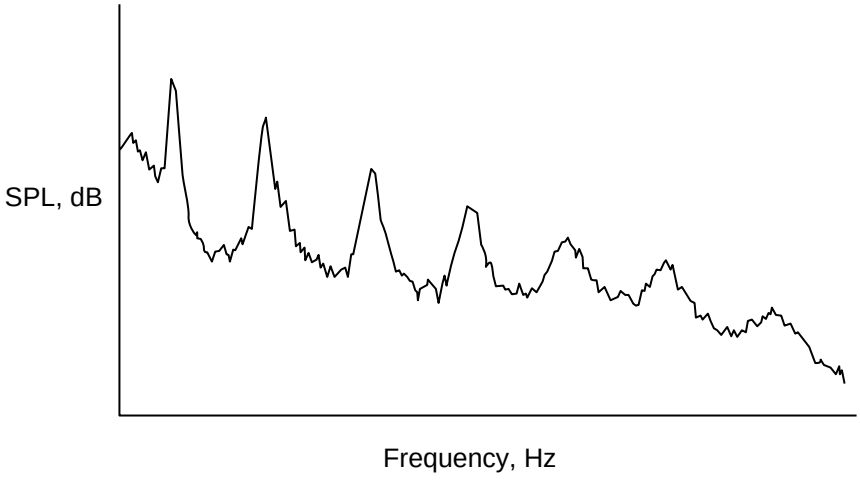

(c) Typical fluctuating pressure spectra.

Figure 1. Open cavity flow field at supersonic speeds (typical for $l/h < 10$).

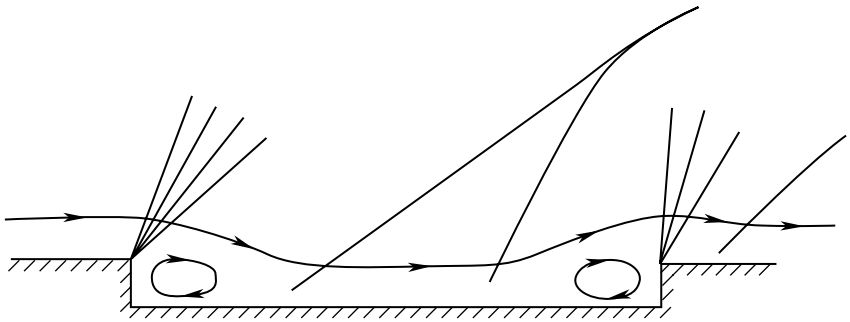

(a) Flow field model.

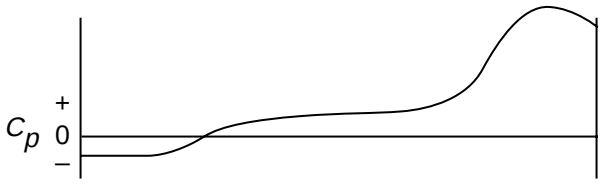

(b) Typical static pressure distribution.

(c) Typical fluctuating pressure spectra.

Figure 2. Closed cavity flow field at supersonic speeds (typical for $l/h > 13$).

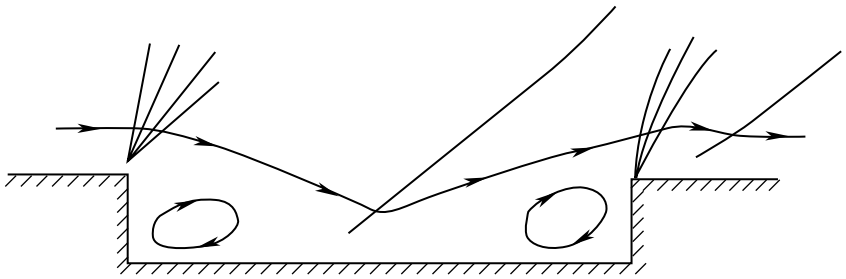

(a) Transitional-closed flow field model.

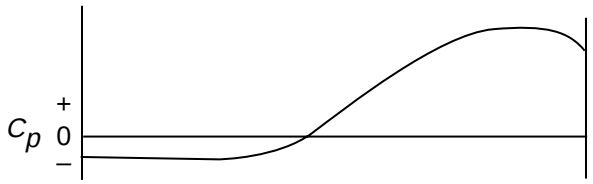

(b) Typical static pressure distribution for transitional-closed flow.

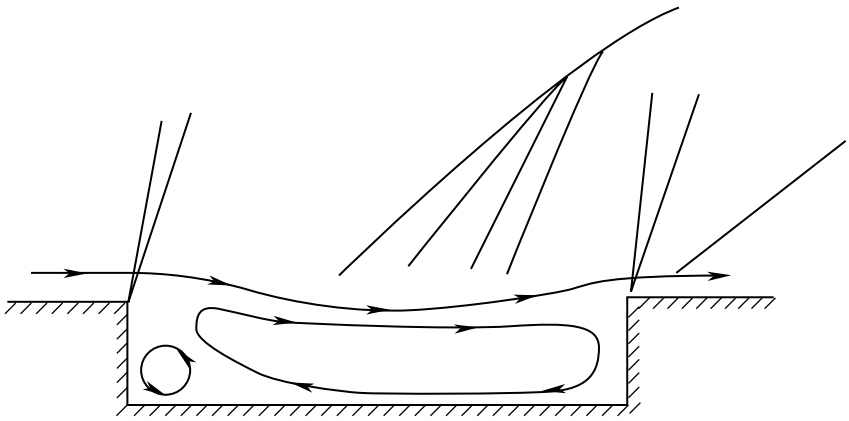

(c) Transitional-open flow field model.

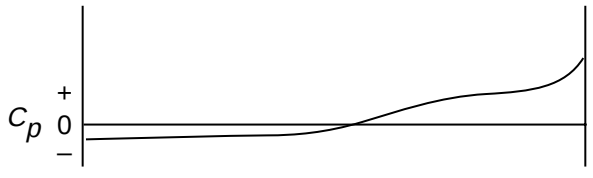

(d) Typical static pressure distribution for transitional-open flow.

Figure 3. Transitional cavity flow fields at supersonic speeds (typical for $10 \leq l/h \leq 13$).

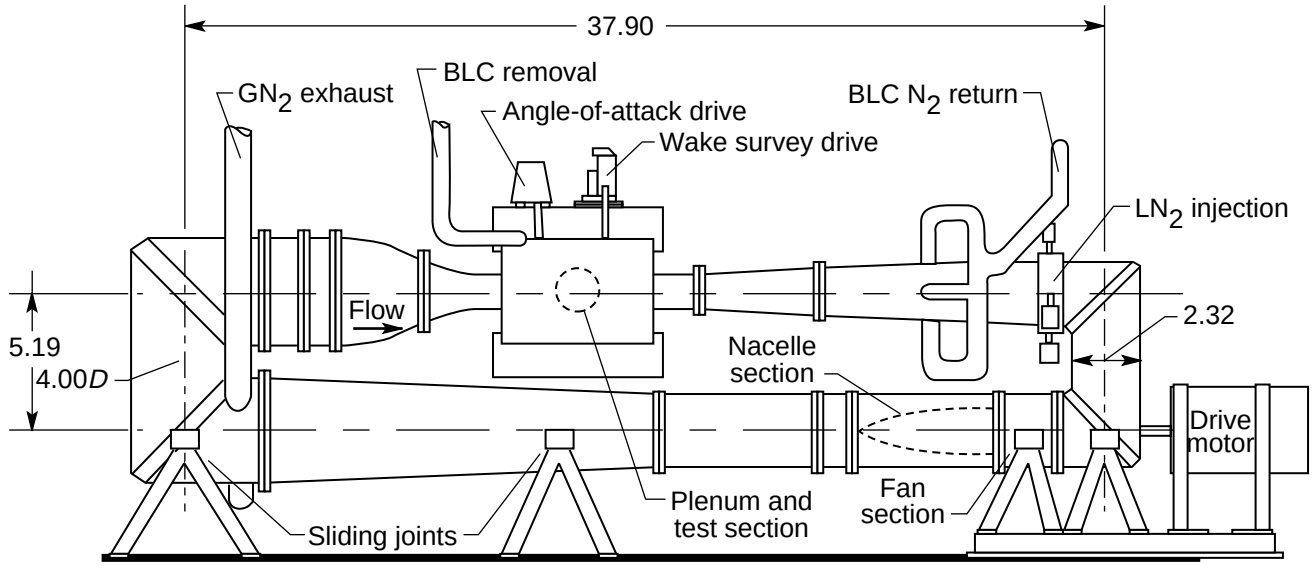

Figure 4. Langley 0.3-m TCT with 13- by 13-in. adaptive-wall test section. Linear dimensions are given in feet.

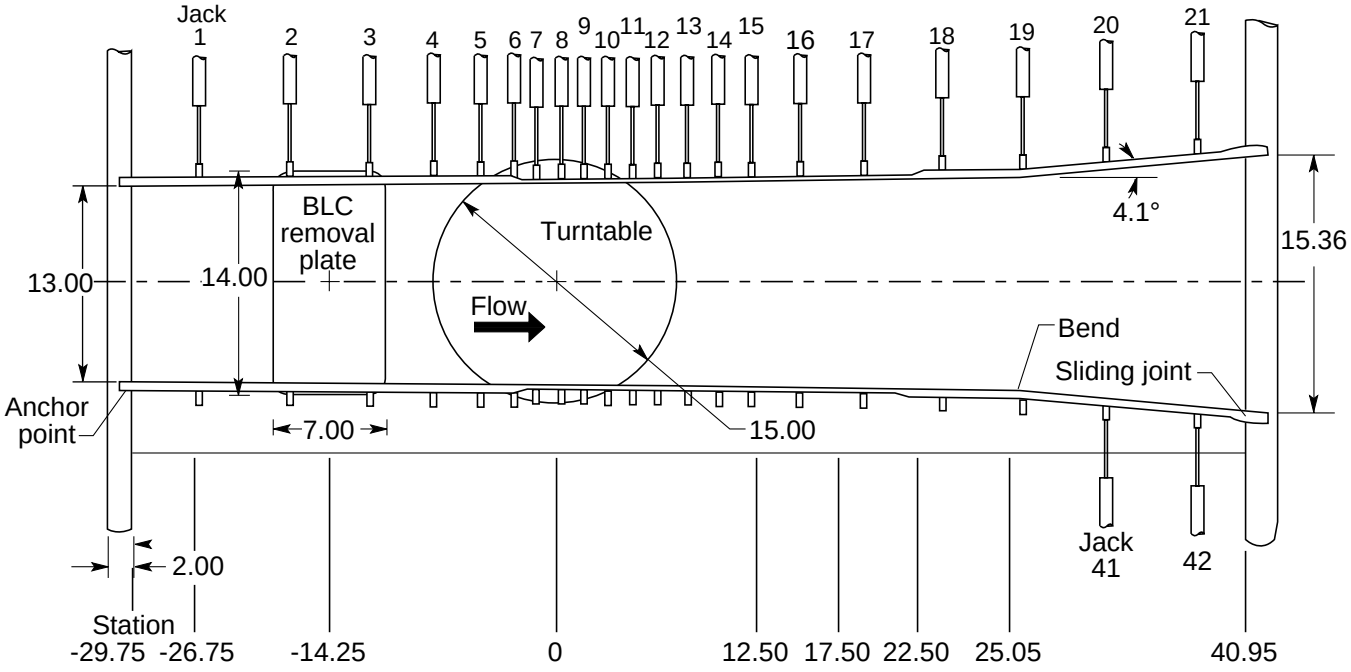

Figure 5. Details of flow region of 13- by 13-in. adaptive-wall test section. Some lower wall jacks are omitted for clarity. All linear dimensions are given in inches.

L-92-23

Figure 6. Interior of 13- by 13-in. test section of the Langley 0.3-m TCT.

L-92-24

Figure 7. Rectangular cavity model prior to installation in sidewall of Langley 0.3-m TCT. Dynamic pressure transducers are shown.

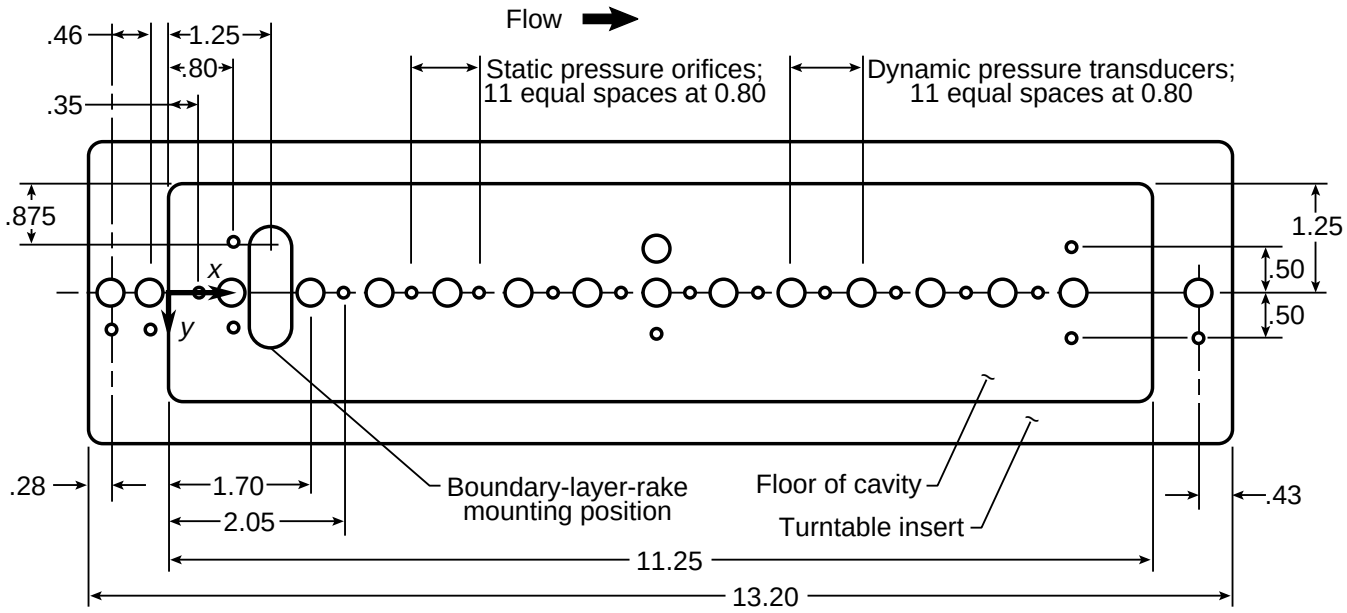

(a) Plan view.

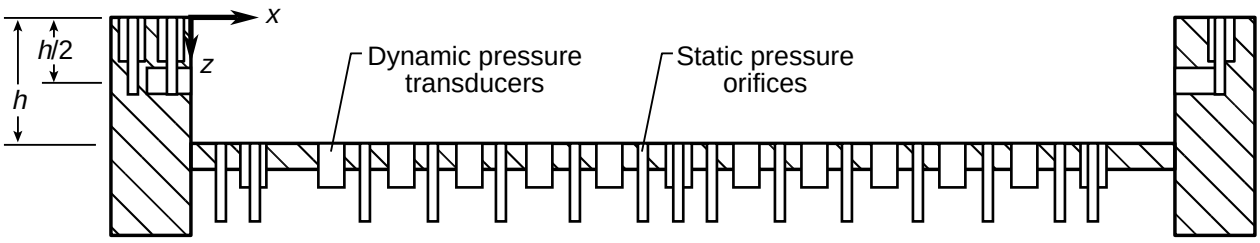

(b) Section side view.

Figure 8. Schematic diagram of instrumented cavity model. All linear dimensions are given in inches.

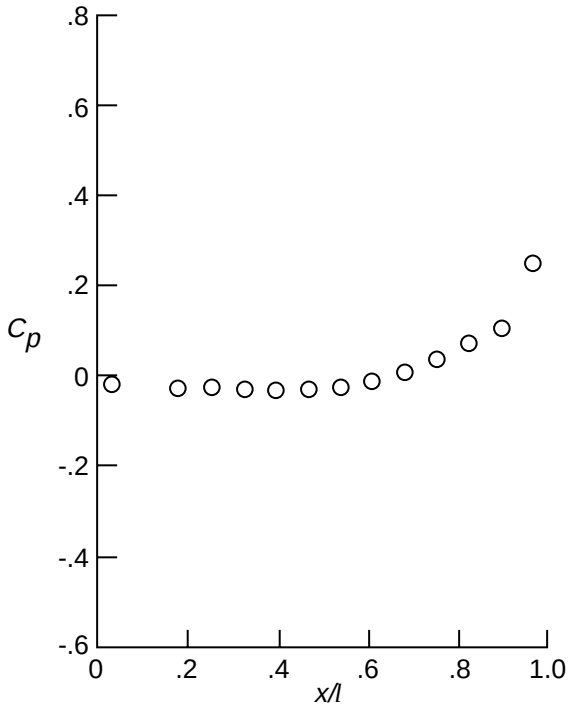

(a) Static pressure distribution.

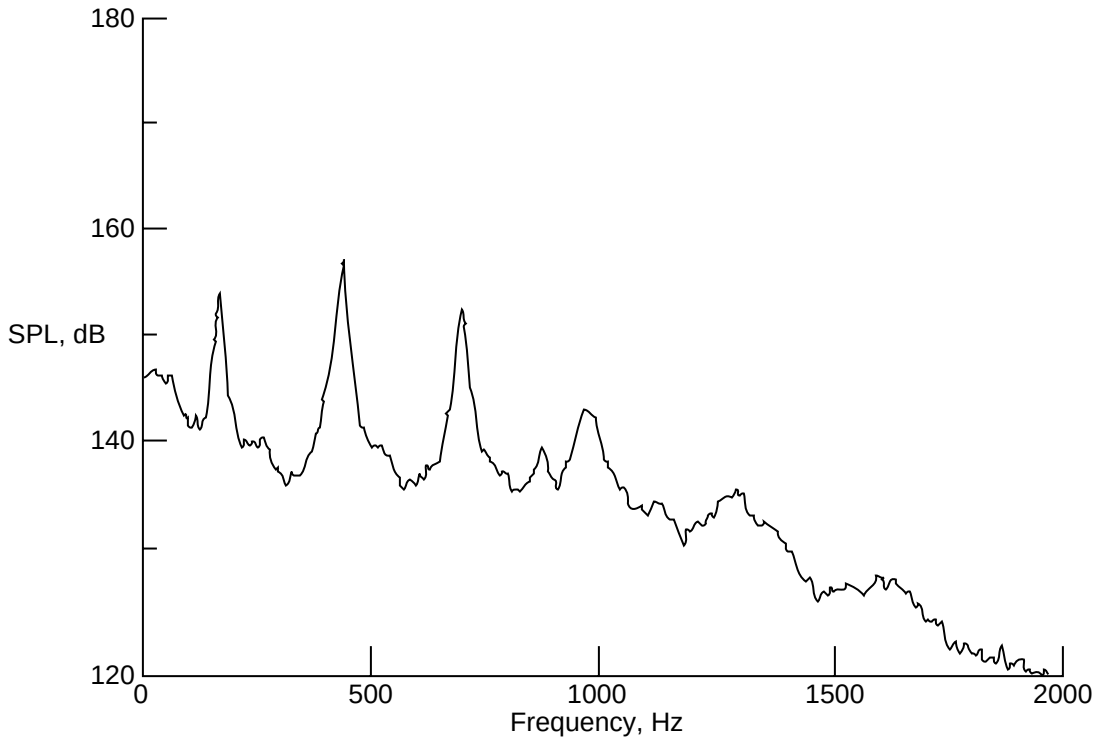

(b) Acoustic spectra measured on forward floor.

Figure 9. Typical pressure data for open cavity flow for $l/h = 4.4, M_\infty = 0.9$, and $\psi = 0°$.

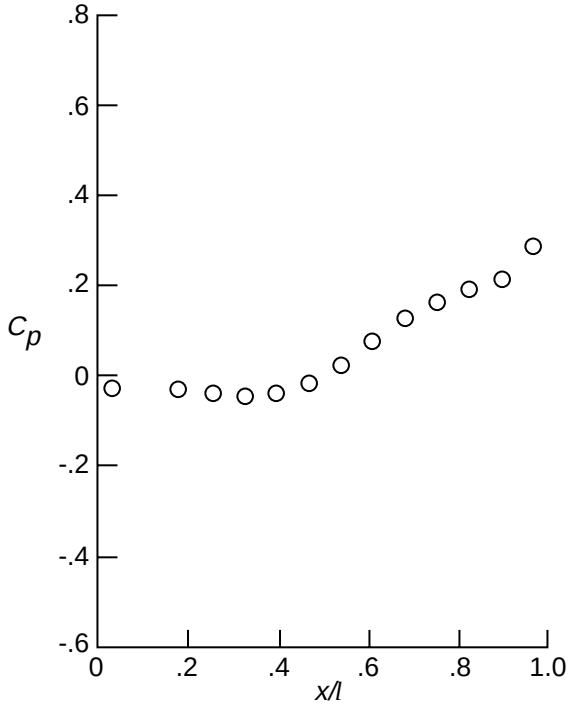

(a) Static pressure distribution.

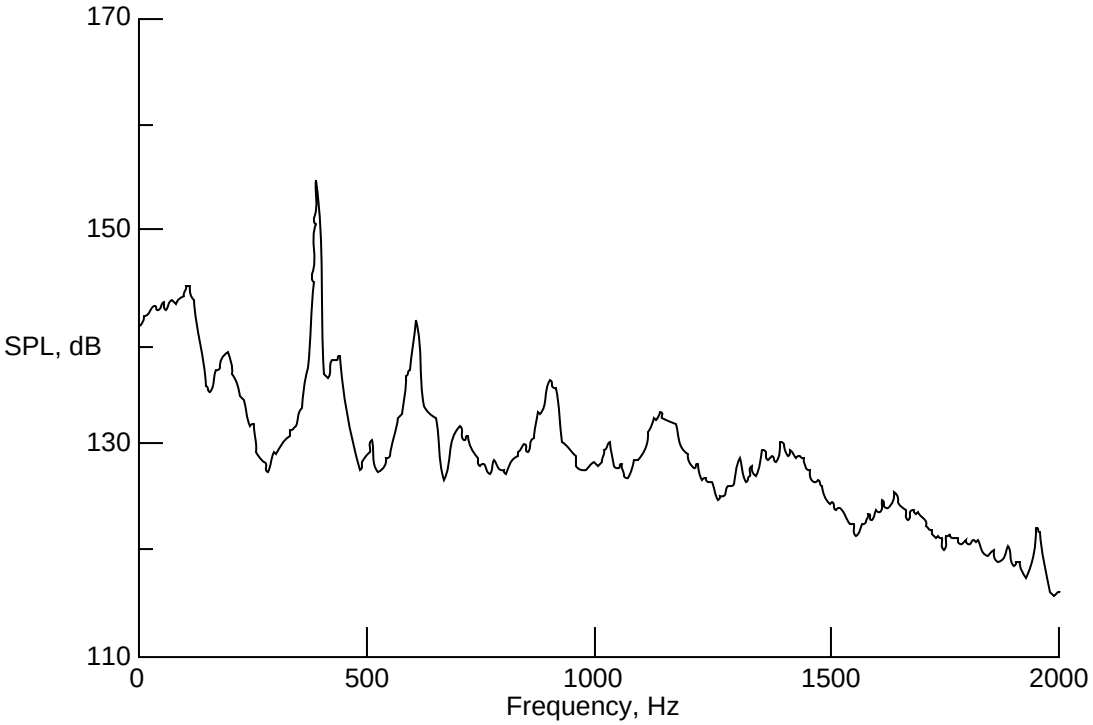

(b) Acoustic spectra measured on forward floor.

Figure 10. Typical pressure data for transitional-open cavity flow for $l/h = 6.7, M_\infty = 0.8$, and $\psi = 0°$.

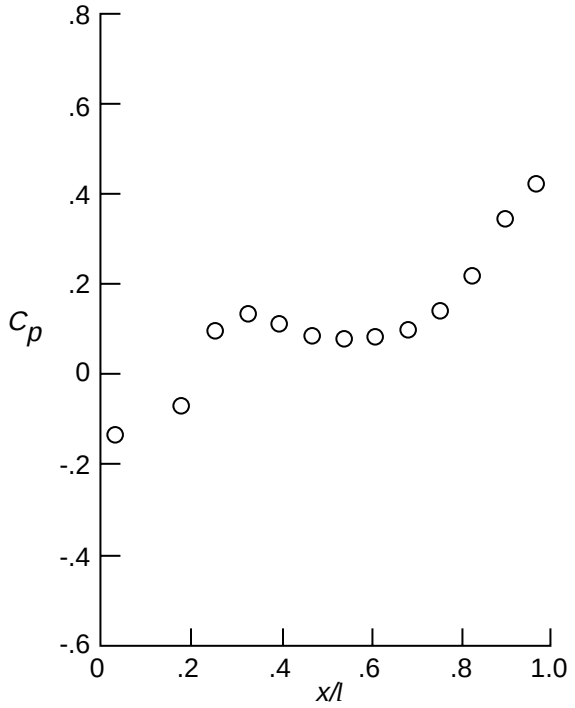

(a) Static pressure distribution for $l/h = 20.0$.

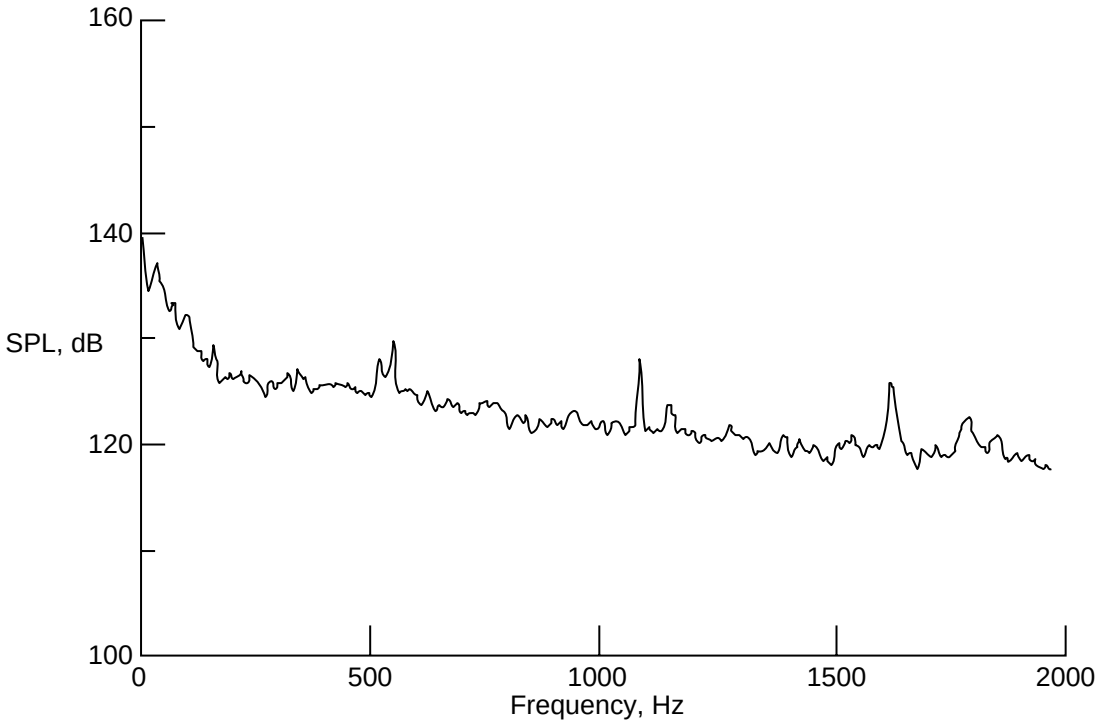

(b) Acoustic spectra measured on forward floor for $l/h = 20.0$. Tunnel fan tones at 519, 1038, and 1557 Hz.

Figure 11. Pressure data for closed cavity flow for $M_\infty = 0.6$ and $\psi = 0°$.

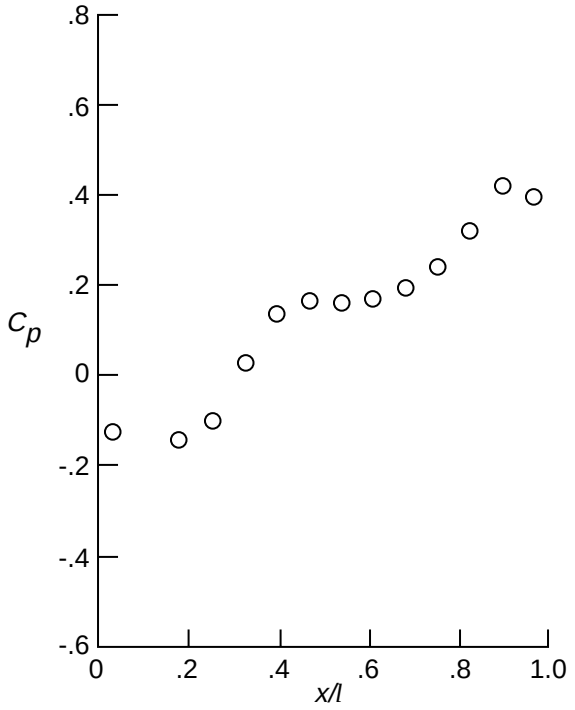

(c) Static pressure distribution for $l/h = 12.67$.

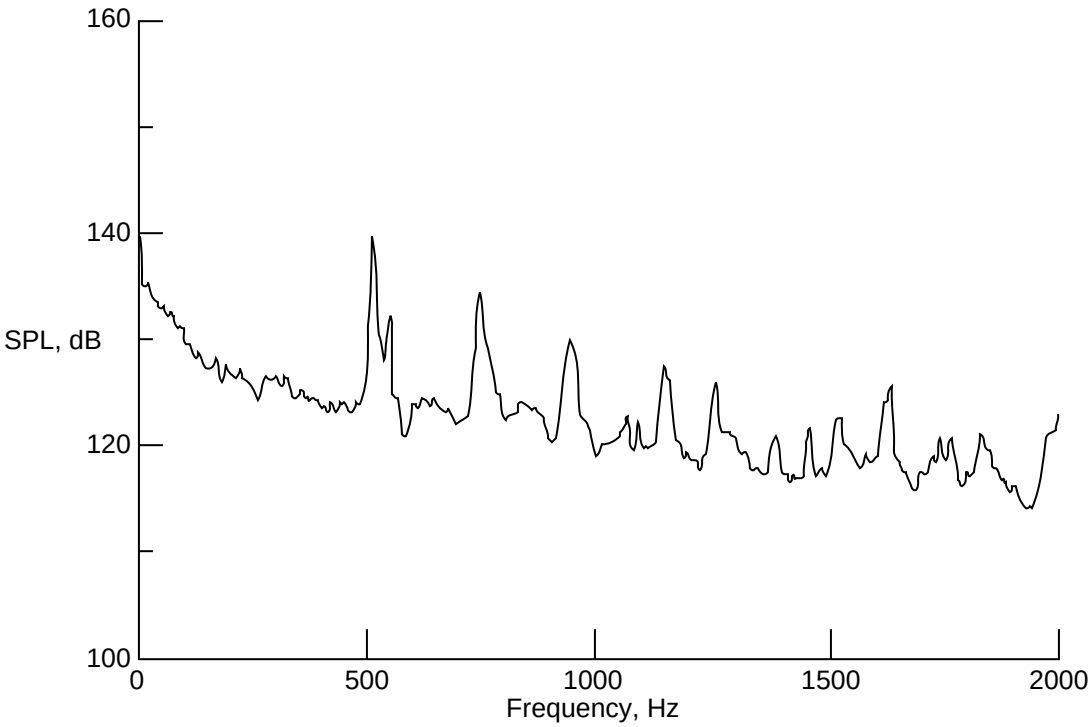

(d) Acoustic spectra measured on forward floor for $l/h = 12.67$.

Figure 11. Concluded.

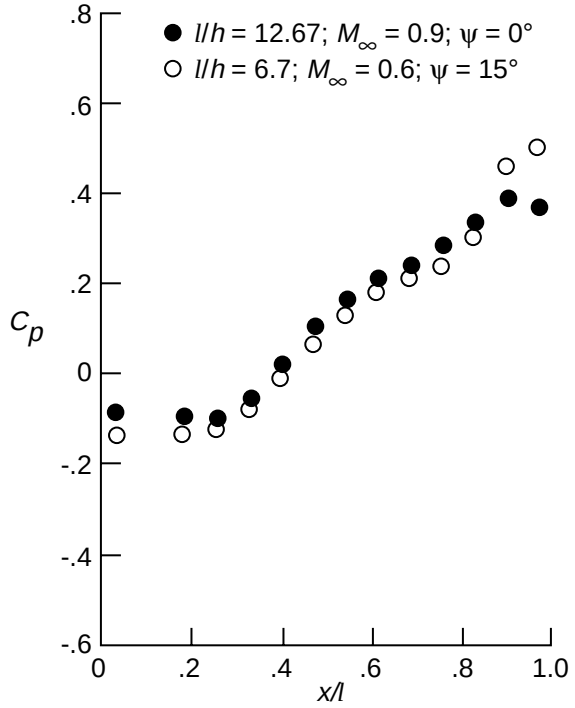

(a) Static pressure distribution.

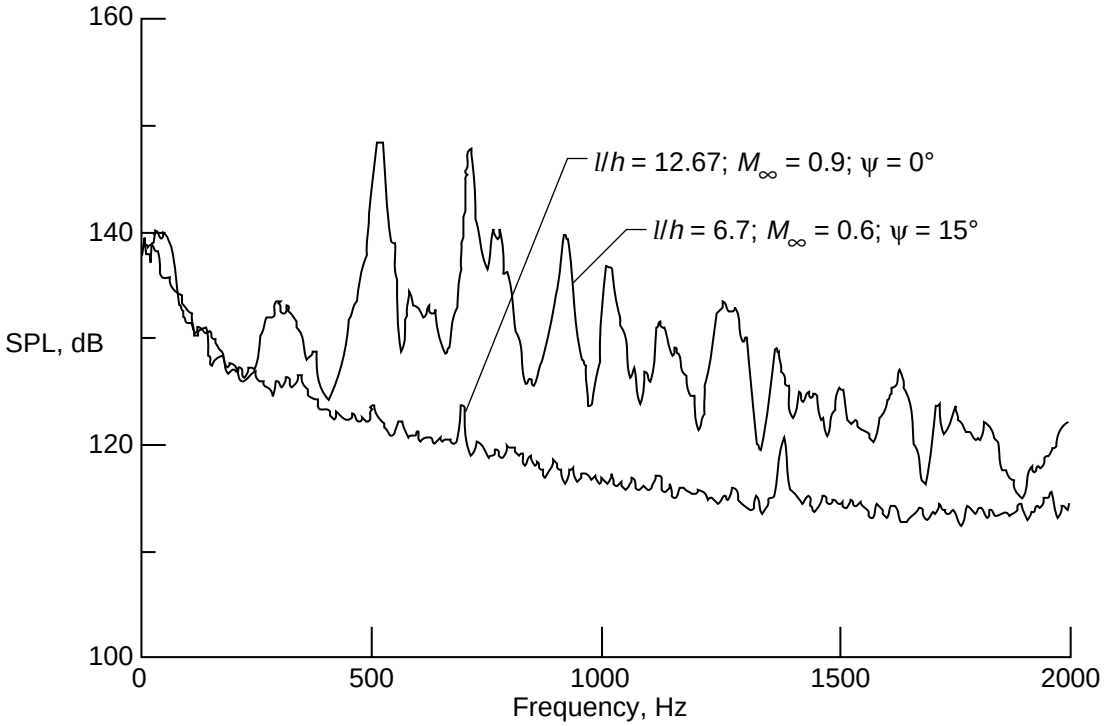

(b) Acoustic spectra measured on forward floor.

Figure 12. Pressure data for two transitional-closed cavity flows.

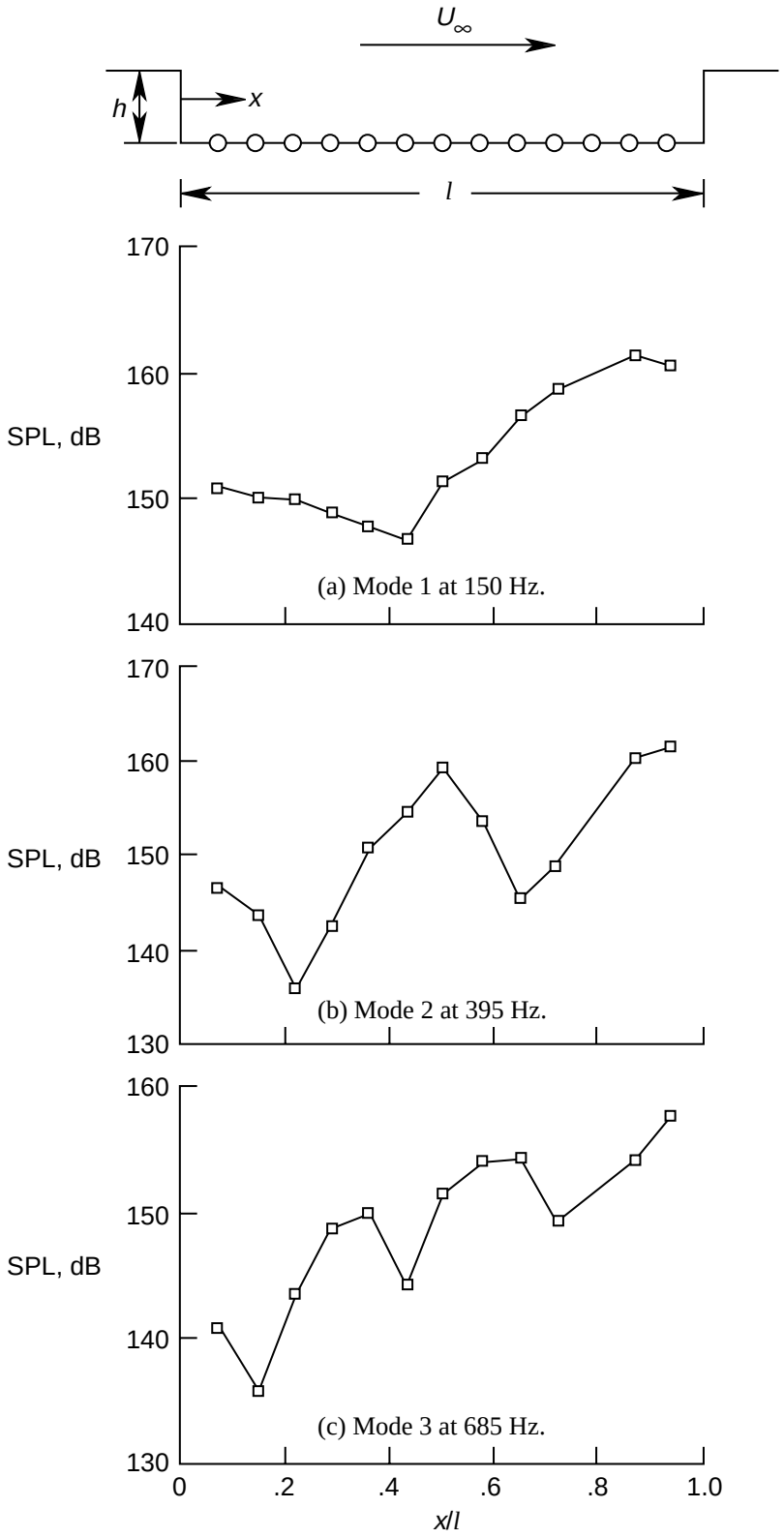

Figure 13. Six mode shapes of a cavity for $l/h = 6.7$ at $M_\infty = 0.9$ and $\psi = 0°$.

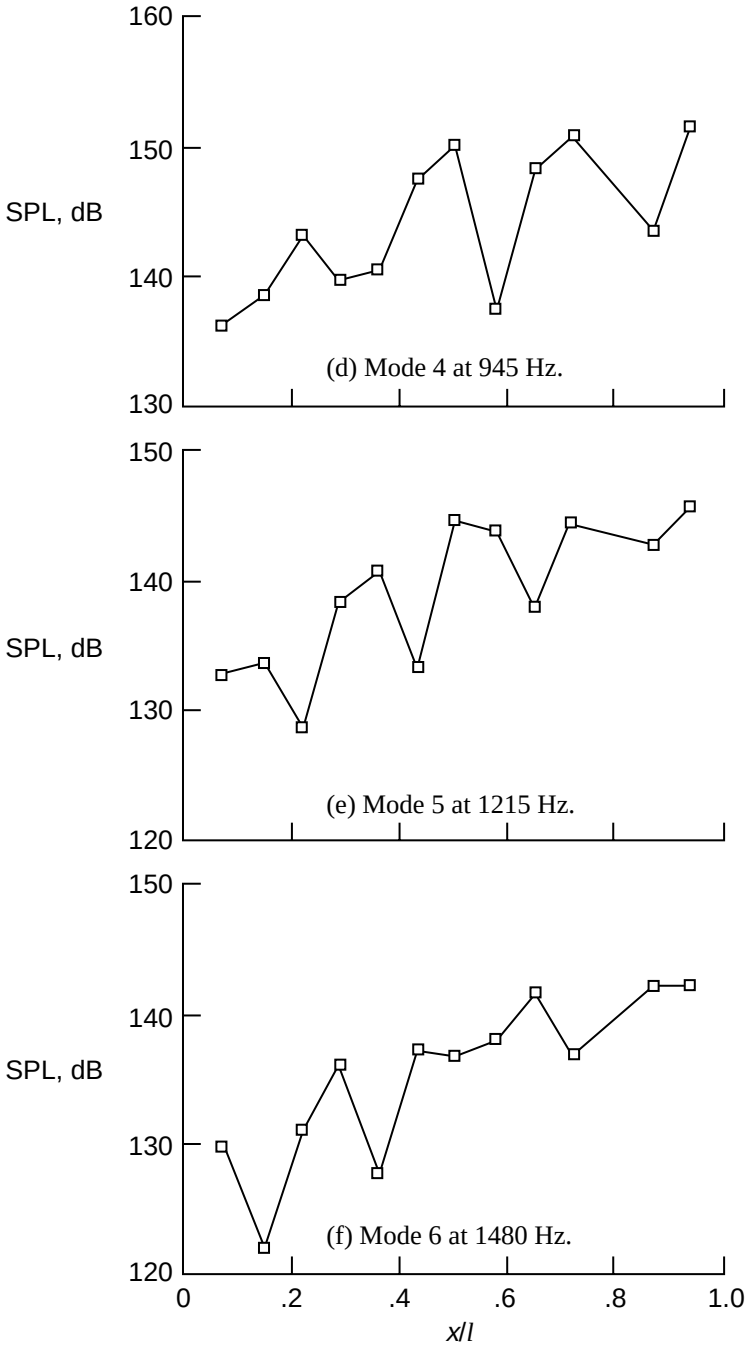

Figure 13. Concluded.

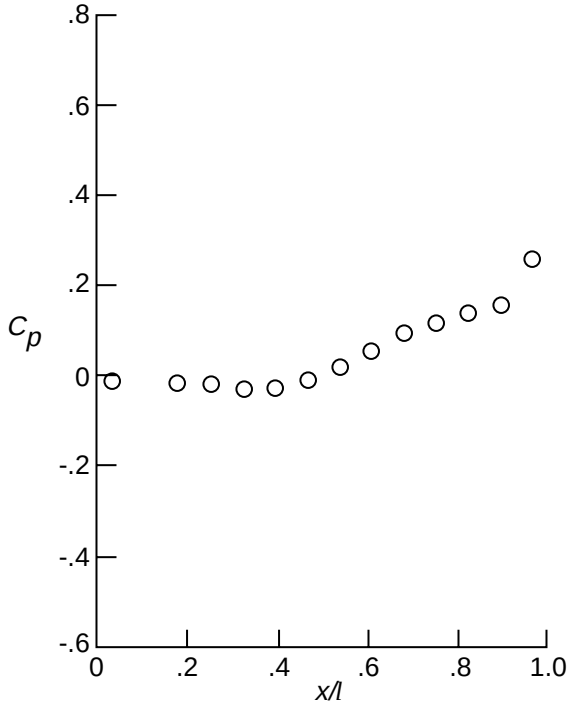

(a) Static pressure distribution.

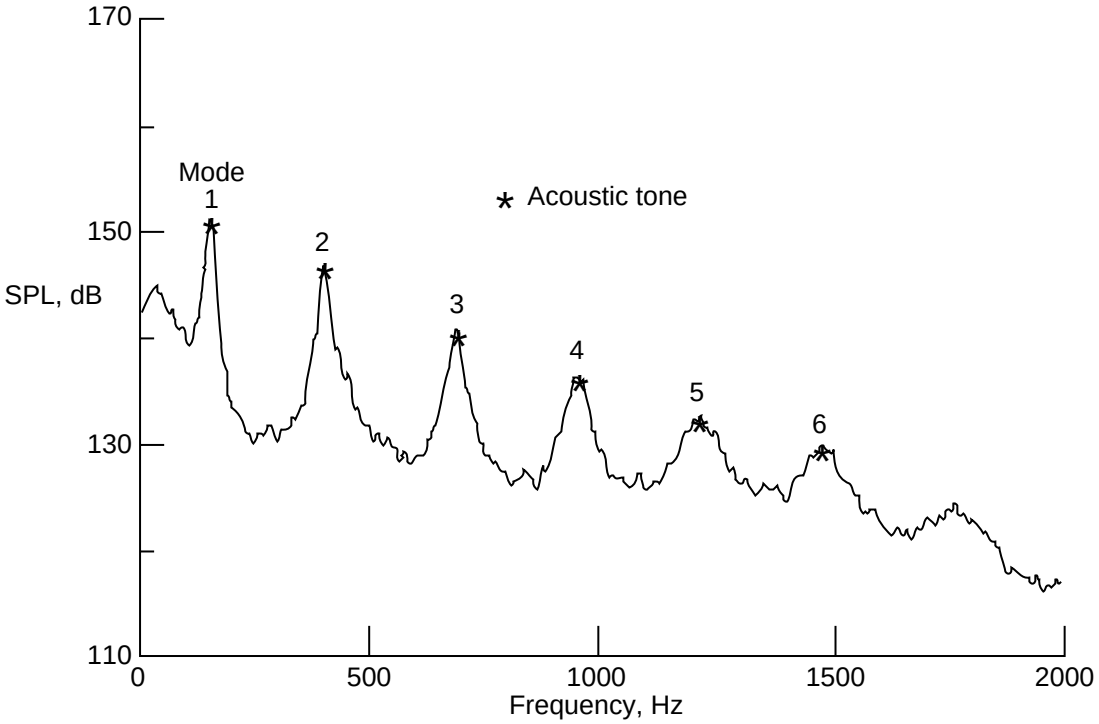

(b) Acoustic spectra measured on forward floor.

Figure 14. Pressure data for $l/h = 6.7$, $M_\infty = 0.9$, and $\psi = 0°$.

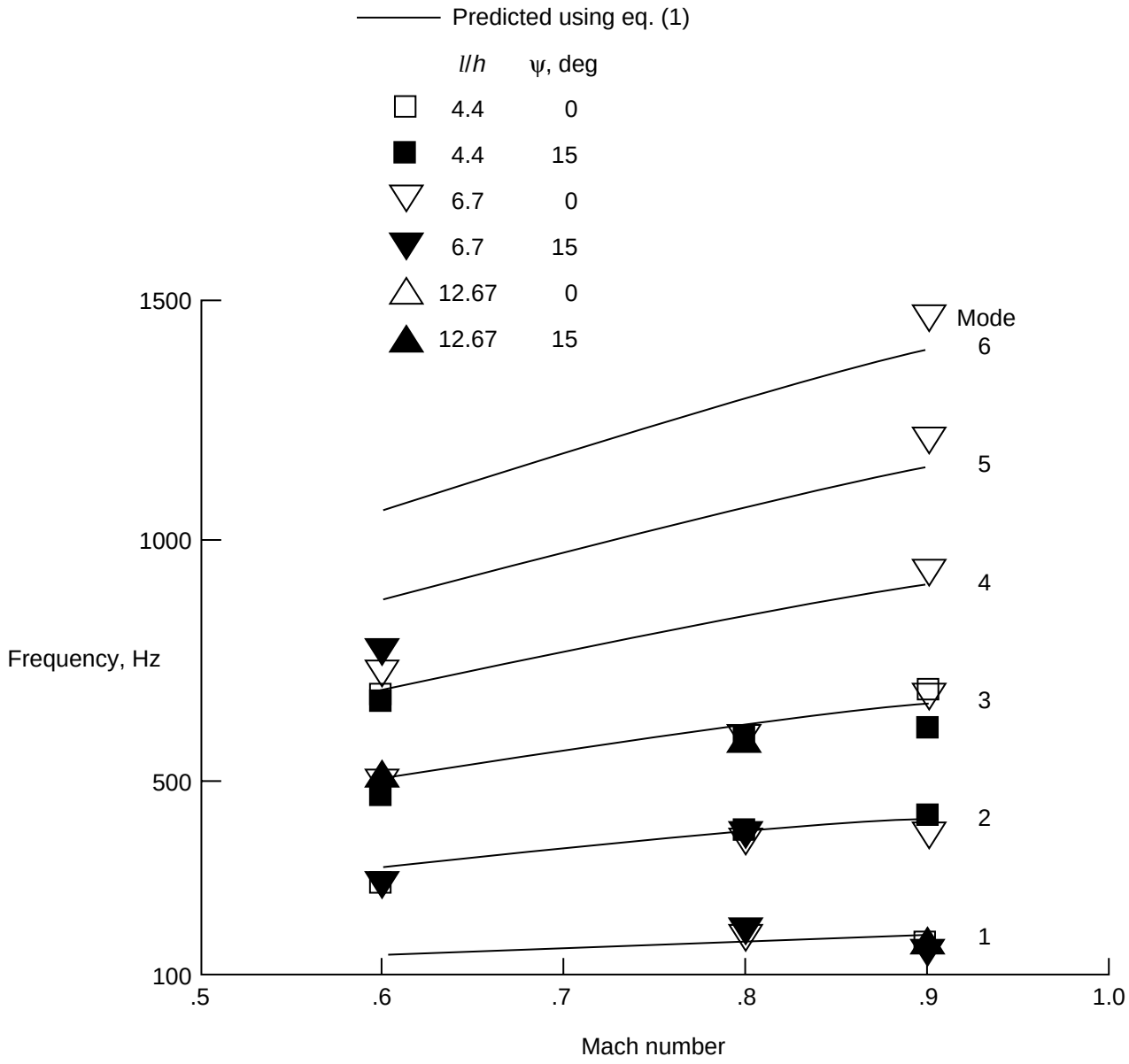

Figure 15. Predicted and observed modal frequencies from tables V and VI, respectively.

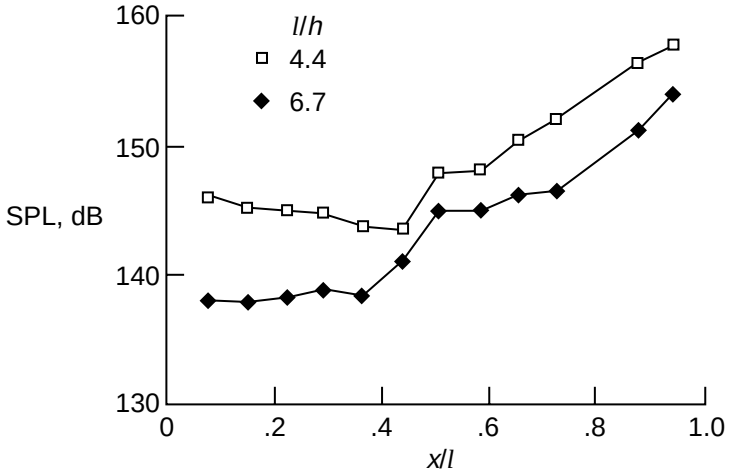

(a) $M_\infty = 0.8$.

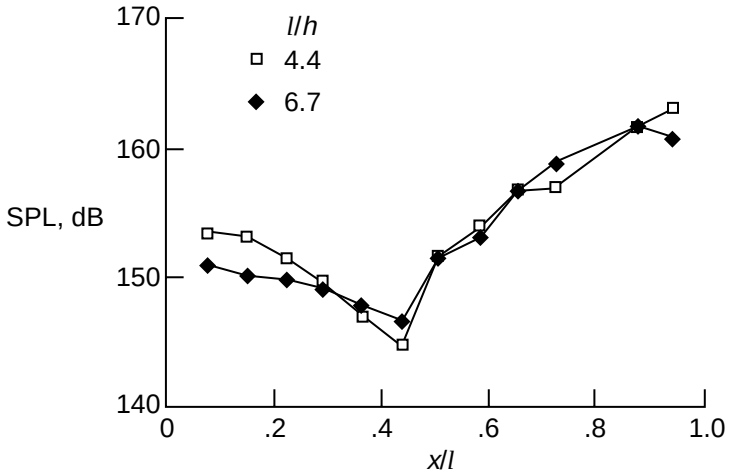

(b) $M_\infty = 0.9$.

Figure 16. Effect of l/h on acoustic mode 1 in cavities at $\psi = 0°$.

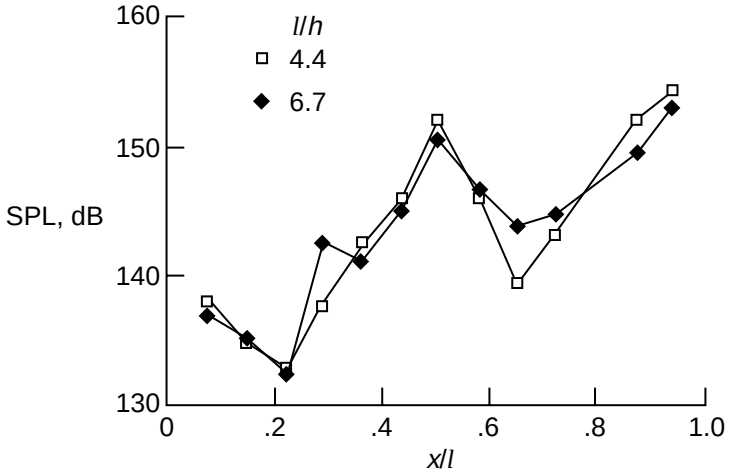

(a) $M_\infty = 0.6$.

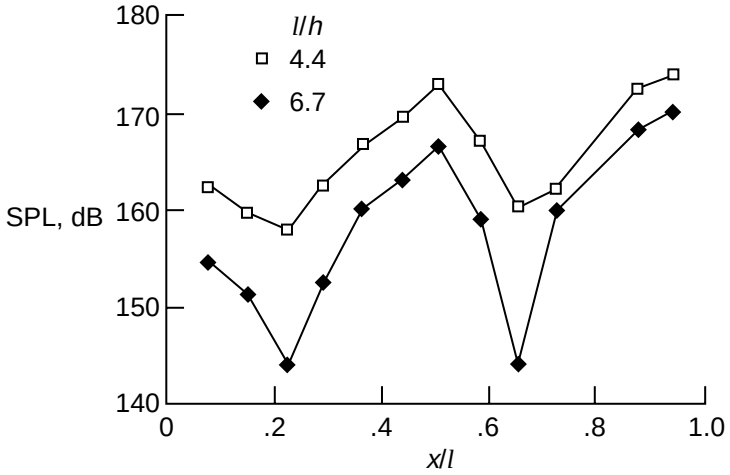

(b) $M_\infty = 0.8$.

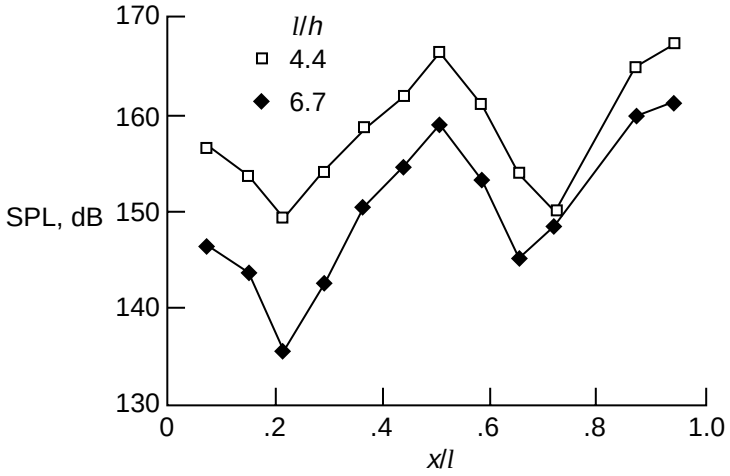

(c) $M_\infty = 0.9$.

Figure 17. Effect of l/h on acoustic mode 2 in cavities at $\psi = 0°$.

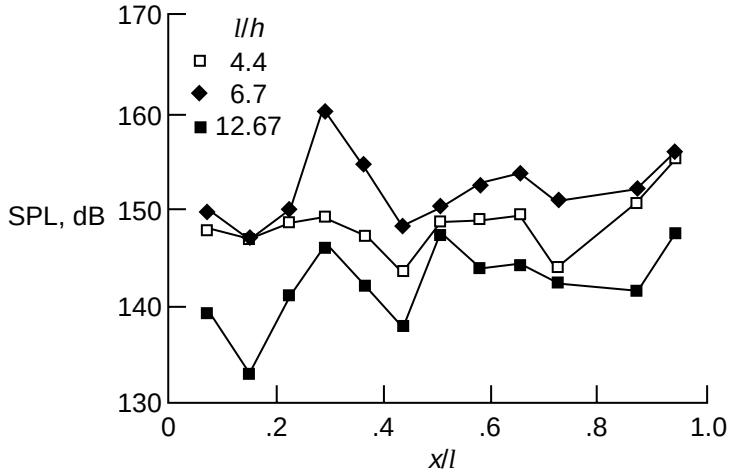

(a) $M_\infty = 0.6$.

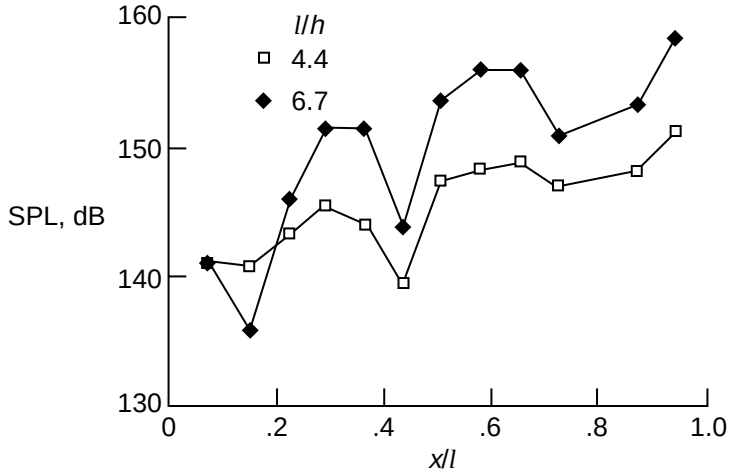

(b) $M_\infty = 0.8$.

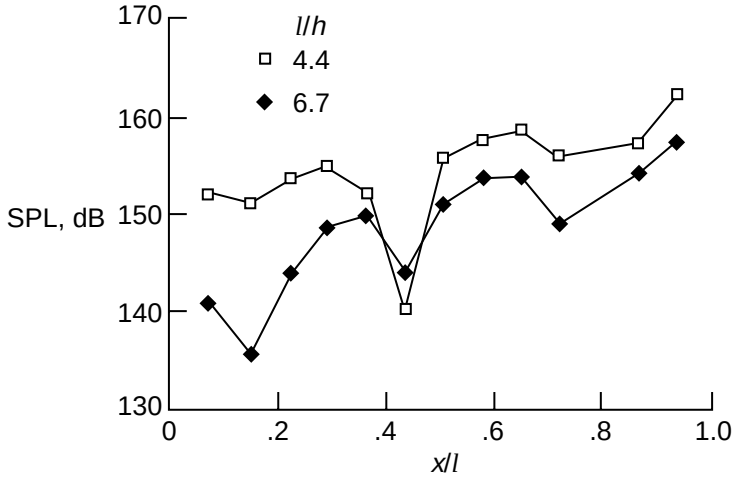

(c) $M_\infty = 0.9$.

Figure 18. Effect of l/h on acoustic mode 3 in cavities at $\psi = 0°$.

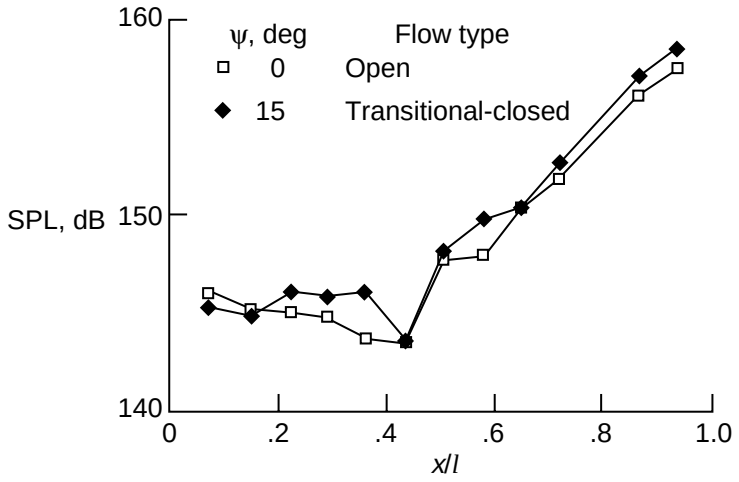

(a) $M_\infty = 0.8$.

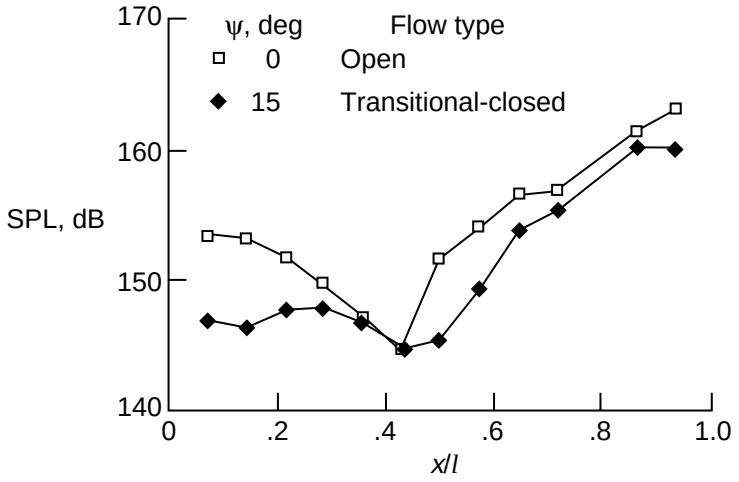

(b) $M_\infty = 0.9$.

Figure 19. Effect of yaw on acoustic mode 1 in cavities with $l/h = 4.4$.

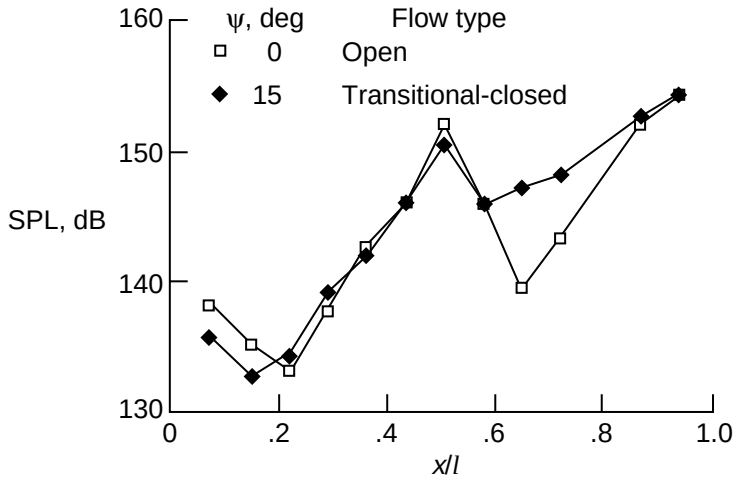

(a) $M_\infty = 0.6$.

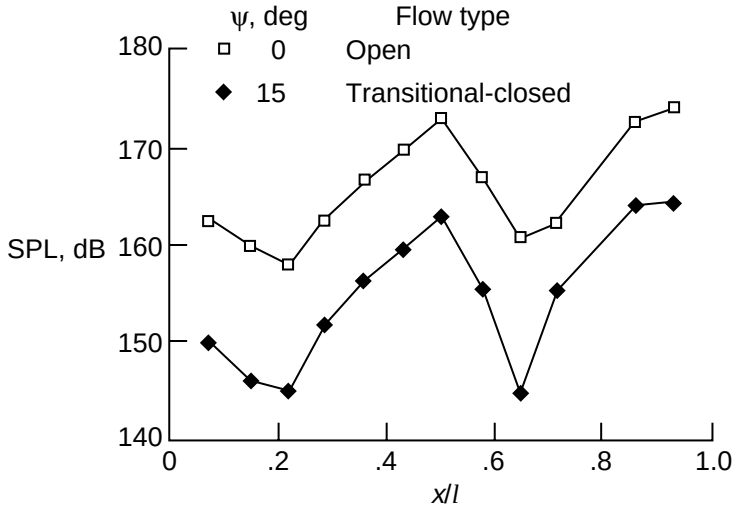

(b) $M_\infty = 0.8$.

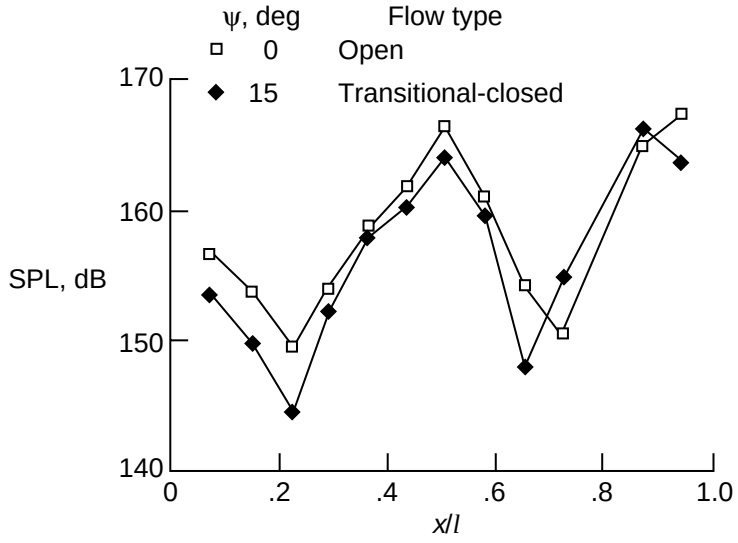

(c) $M_\infty = 0.9$.

Figure 20. Effect of yaw on acoustic mode 2 in cavities with $l/h = 4.4$.

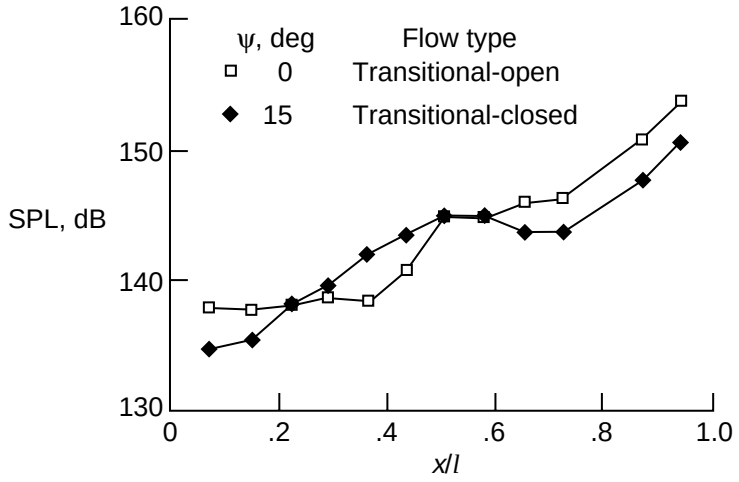

(a) $M_\infty = 0.8$.

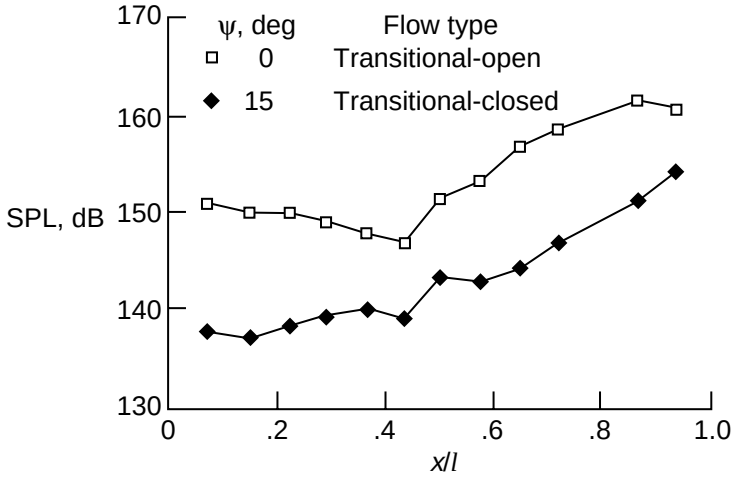

(b) $M_\infty = 0.9$.

Figure 21. Effect of yaw on acoustic mode 1 in cavities with $l/h = 6.7$.

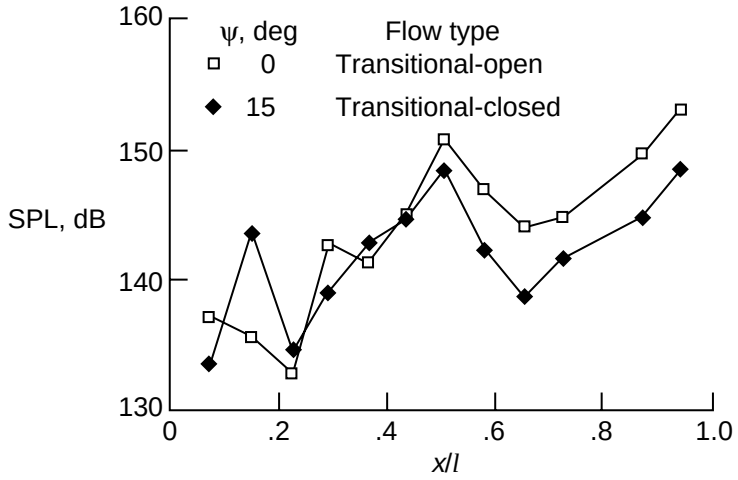

(a) $M_\infty = 0.6$.

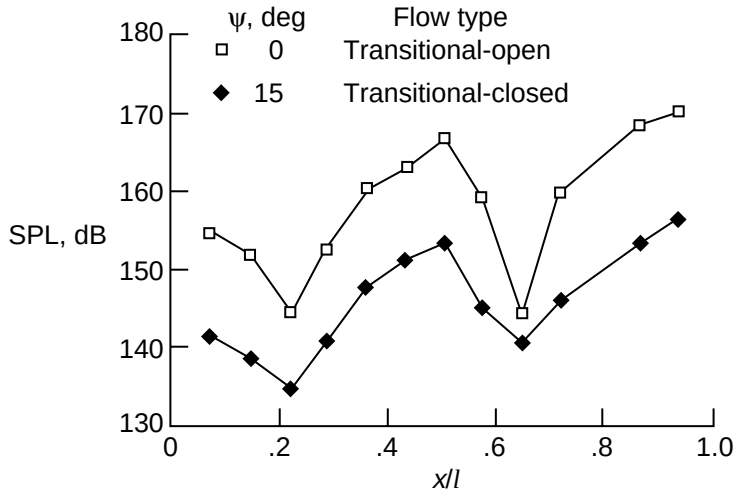

(b) $M_\infty = 0.8$.

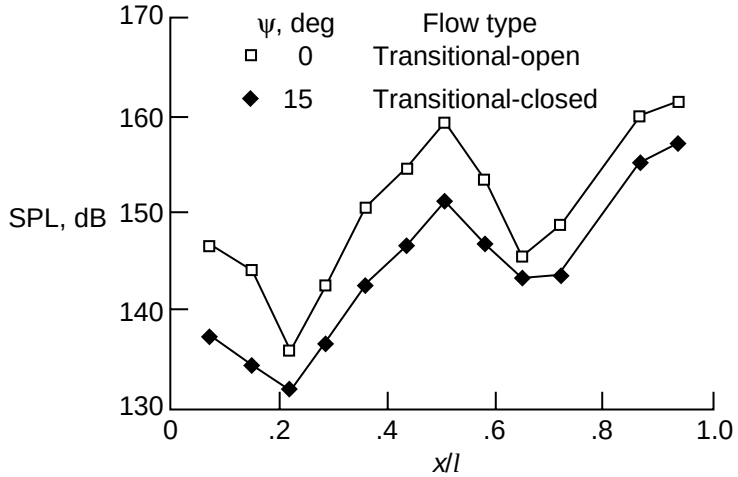

(c) $M_\infty = 0.9$.

Figure 22. Effect of yaw on acoustic mode 2 in cavities with $l/h = 6.7$.